Two-body abrasive wear of electroless nickel composite coatings

C. Subramanian and E. Pallotta

Ian Wark Research Institute, The University of South Australia, The Levels, South Australia 5095, Australia

Received 31 January 1996; accepted 19 March 1996

The two-body abrasive wear of electroless nickel (EN), EN–silicon carbide, and EN–alumina composite coatings have been investigated using a scratch test with a diamond indenter. The coatings were heat treated at temperatures of 100–500°C. The hardness of the coatings increased with heat treatment temperature from 500 HV100 for the as-deposited condition to 1008 HV100 when fully hardened. Scratch testing showed that the as-deposited coating had scratch tracks with a high degree of plasticity, signs of microploughing and tensile cracking and was characterised as a ductile failure. On the other hand, the heat-treated coatings showed chipping and cracking on the edge of the scratch tracks, failing in a brittle manner. The heat-treated EN–silicon carbide coatings, however, exhibited no cracking nor chipping, believed to be due to its higher fracture toughness than the other heat-treated coatings, attributable to its lower phosphorus content. The volume of material removed from the silicon carbide scratch track was 1/3 of the volume removed from the steel substrate at a 20 N load, and showed the best wear/scratch resistance of any of the coatings tested.

Keywords: abrasion; electroless nickel; composite coatings; wear; scratch testing; two-body abrasion

1. Introduction

Electroless nickel (EN) plating is a process used to deposit nickel without the use of an electric current by the autocatalytic chemical reduction of nickel ions by the hypophosphite ion. The coatings produced by this process are not pure nickel but an amorphous nickel–phosphorus deposit. The phosphorus content of the deposit is an important variable as it affects its physical (e.g. density, electrical conductivity) and mechanical properties (hardness, strength, and ductility) which, in turn, influence the wear and corrosion behaviour of the coating. Electroless coatings can be used to coat polymers and other non-conducting materials, and have excellent uniformity and throwing power over the substrate because the process is autocatalytic. The coatings can be soldered or brazed, enabling them to be used in electronics and other general engineering applications. The main limitations of the process are the high cost of chemicals and the slower plating rate compared to electrolytic processes [1].

The electroless nickel deposits can be precipitation hardened by heat treatment, whereupon the matrix becomes crystalline. The variation of hardness with heat-treatment temperature shows that the hardness changes very little when the annealing temperature is below 250°C, but above this temperature it changes abruptly. The alloys reach a maximum hardness at a certain temperature, above which hardness falls gradually. The increase in hardness is due to the formation of the hard intermediate phase Ni_3P. The higher the phosphorus content, the more Ni_3P phase forms during the heat treatment, which consequently results in a higher peak hardness value. The hardness drop at higher temperatures is attributed to the Ostwald ripening process [2,3].

Hard or soft particles (e.g. alumina, diamond, silicon carbide or PTFE (polytetrafluoro ethylene) can be incorporated into electroless nickel coatings typically in the range of 20–30% particles by volume. The particles are carefully sized and are normally 1–3 μm in diameter [4,5]. No molecular bond is established between the particles and the metal matrix. The composite is developed mechanically by the effect of particle settling and impingement upon the surface of the workpiece and subsequent particle envelopment by the matrix.

The primary use of electroless nickel composite coatings is in applications requiring resistance to wear, especially abrasion. All composites tested, regardless of the particulate incorporated, showed a substantially improved wear resistance over the electroless nickel coating without any particulate matter. These improvements in wear resistance are well demonstrated by many workers [8–10]. All workers, however, concluded that electroless coatings provide an appreciably higher wear resistance than electrodeposited nickel; and are adequate for many engineering applications [7,12,13].

Gawe has shown that the dominant wear mechanism encountered when electroless nickel slides against most metal surfaces is adhesive wear which can be reduced by heat treatment of the coating [6–8]. In cases of heavy gouging, however, the dominant wear mechanism is most likely to be abrasive, and heat treatment in this case would most likely cause a decrease in the wear resistance due to a decrease in fracture toughness.

In the present study, the plating procedure of electroless nickel coatings, to produce electroless nickel composite coatings with silicon carbide and alumina particulates on a mild steel substrate, were examined and the wear resistance of the coatings was evaluated by scratch testing.

2. Experimental

Rectangular mild steel substrates with dimensions of 50 × 25 × 2 mm were grit blasted to remove corrosion products and to produce a rough surface to improve coating adhesion. The test pieces were then ultrasonically cleaned in a detergent

solution for 15 min, ultrasonically degreased in ethanol for 15 min and subsequently hot-air dried just prior to plating.

The electrolytes were prepared by dissolving 24 g of solid sodium hypophosphite and 20 g of solid nickel chloride in 500 ml of deionised water in separate beakers. Both solutions were then heated until they reached 60°C and were then mixed together in one beaker forming 1 ℓ of plating solution. Immediately, 1 mg of lead ions was added to stabilise the bath, followed by 10 g of silicon carbide or alumina particles. A set of four test substrates, suspended via nylon string, was immersed in the plating solution.

During the plating process, a magnetic stirrer was used to circulate the plating solution and the beaker sealed with plastic wrap to minimise moisture loss via evaporation. The pH and the bath temperature were monitored, the pH being controlled by adding ammonium hydroxide to neutralise the hydrogen ions produced by the reaction, and the temperature by adjusting the setting on the hotplate. The pH was maintained at 4.5 and the temperature at 95°C, the plating time was approximately 2 h or until the bath began to catalytically decompose.

The coated test pieces were heat treated in a neutral salt bath at various temperatures between 100 and 500°C for 1 h. Hardness measurements were carried out using a Leitz microhardness tester under a load of 1 N.

Two-body abrasive wear behaviour of the electroless nickel coating was evaluated using a VTT scratch tester (VTT Technology, Espoo, Finland). It consists of a 0.2 mm radius, diamond-tipped indenter, which is in contact with the test samples on a moving table at a fixed velocity. The applied load onto the diamond indenter can be fixed or varied continuously by an electric motor. During the test, frictional force can be recorded continuously by a set of strain gauges attached to the table. Scratching testing has been widely used in the evaluation of the adhesion of hard coatings such as TiN to the substrates. In the present investigation, the scratch tester was used as a two-body abrasion tester. The scratch-abrasion testing of the coated samples was carried out under different (fixed) loads. The signals of the normal load and the tangential force were collected using a computerised data acquisition system for further analysis.

The scratch track was profiled using a Surtronic 3+ profilometer (Rank Taylor Hobson), and the amount of the coating material displaced from the coating was determined. A Camscan CS44FE scanning electron microscope (SEM) with an energy dispersive X-ray spectrometer (EDS) was used to analyse the scratch tracks and the microstructure of the coatings.

3. Results and discussion

3.1. MICROSTRUCTURE

The scanning electron micrographs of the as-deposited EN, EN–silicon carbide, and EN–alumina composite coatings are shown in figs. 1–3, and are abbre-

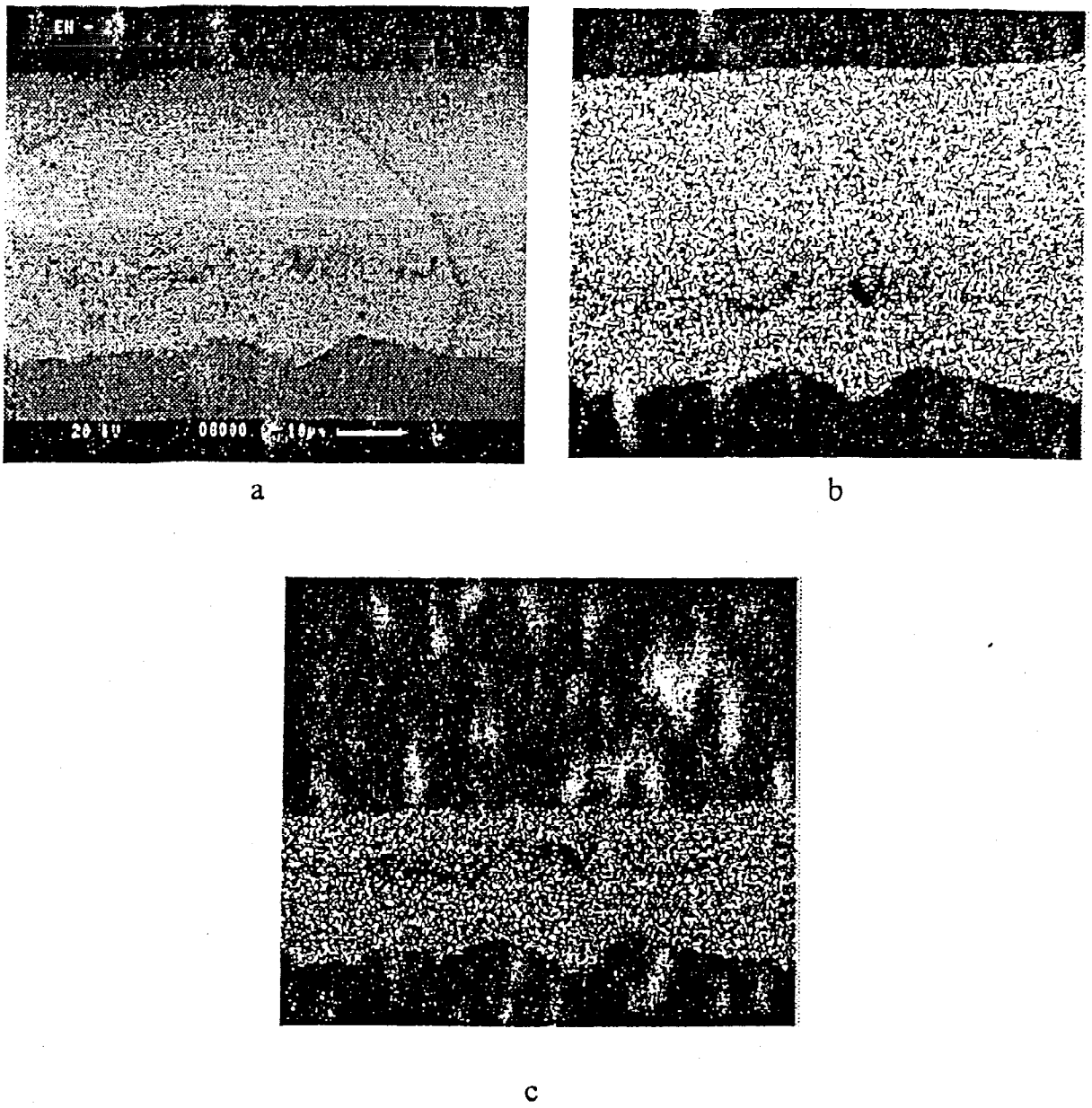

Fig. 1. SEM of a cross section of the electroless nickel coating (a); EDS map for Ni (b), P (c).

viated to EN, ENSI and ENAL, respectively. Numbers that follow these abbreviations refer to the temperature at which the coating was heat treated, e.g. ENAL400 refers to an electroless nickel alumina coating heat treated at 400°C for 1 h.

Table 1 shows the composition of various coatings obtained from quantitative analyses (using SEM-EDS) of the coating surfaces. The weight percentage of iron detected gives some idea of the coating thickness, i.e. the thicker the coating the smaller the weight percent of iron detected in the qualitative analysis (see table 1).

The volume fractions of silicon carbide and alumina were 20 and 8% in the ENSI and ENAL coatings, respectively. The interparticle spacing was ca. 4 μm as

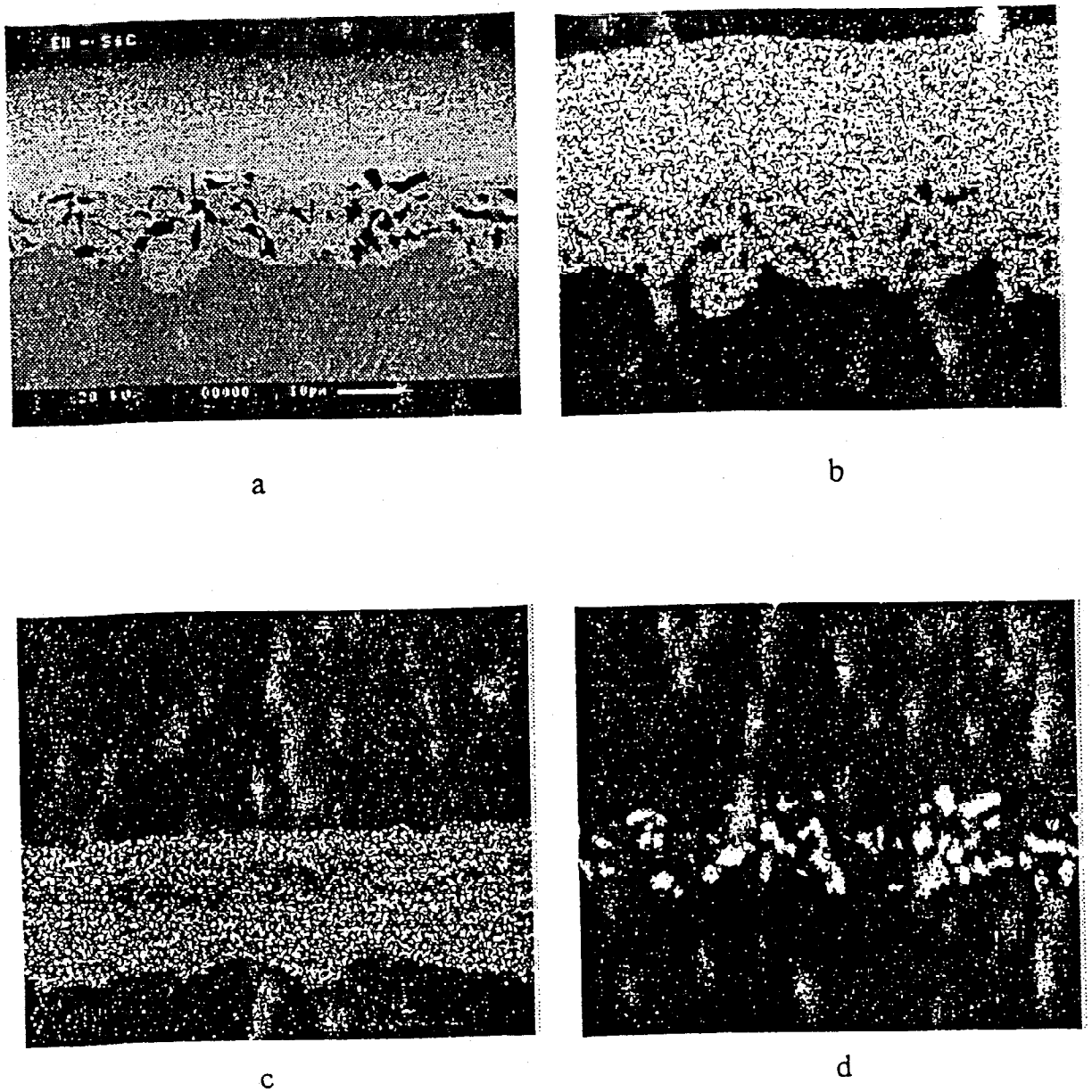

Fig. 2. SEM of a cross section of the electroless nickel–silicon carbide composite (a); EDS map of Ni (b), P (c), Si (d).

estimated from figs. 2 and 3. The thickness of the EN, ENSI, and ENAL coatings are 15, 12, and 18 μm, respectively. The absence of porosity and cracking at the coating/substrate interface visually indicates that the coating adhesion for all three coatings in the as-deposited condition is good, which can be attributed to grit blasting of the substrate to increase the surface roughness and sites for mechanical interlocking. The adhesion of alumina particles to nickel particles is believed to be caused by electrostatic forces of absorption between nickel and alumina, and the magnitude of these forces is believed to be much higher than the mechanical interlocking forces [14].

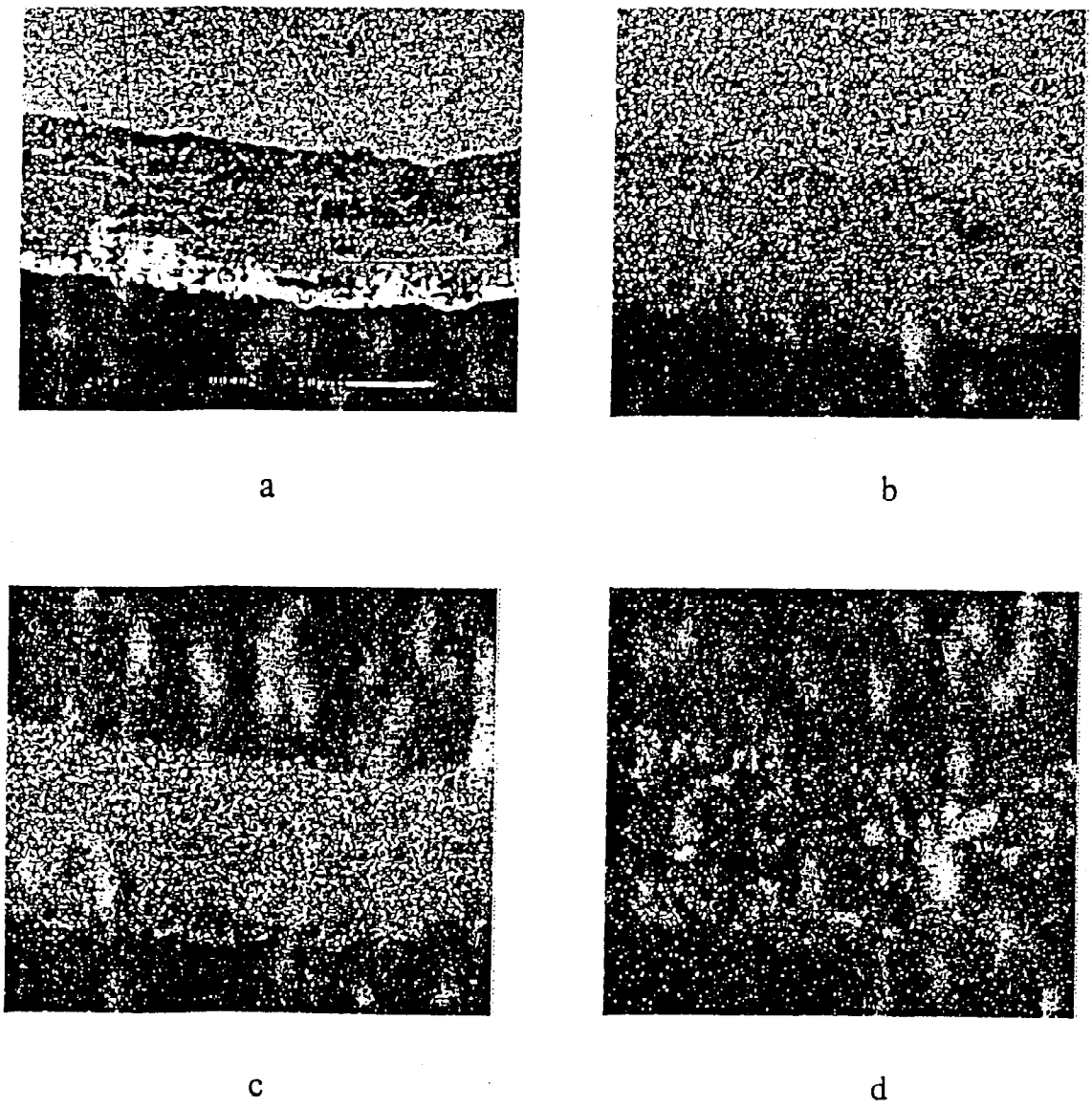

Fig. 3. SEM of electroless nickel alumina composite coating (a); EDS map of Ni (b), P (c), Al (d).

3.2. HARDNESS TESTING

Fig. 4 shows the hardness of all samples as a function of heat treatment temperature (for 1 h). All coatings showed a trend of increasing hardness with increasing temperature, up to a temperature of 400°C, followed by a drop in hardness. The coatings have a hardness of approximately 500 HV100 in the as-deposited condition, and reach a maximum hardness of 1008 HV100, when heat treated to 400°C. At temperatures between 450 and 500°C, the coatings softened and the hardness values decreased to approximately 800 HV100 (still much harder than the coatings in the as-deposited state).

Table 1
Energy dispersive X-ray analysis of the surface of the electroless nickel deposits

Composition (relative) (wt%)	As-deposited	Alumina composite	Silicon carbide composite
Fe	0.95	0.42	1.12
Ni	90.03	85.9	76.05
P	9.02	10.43	8.24
Al	–	3.26	–
Si	–	–	13.60
Ca	–	–	1.00
total	100	100	100

The general trend of increasing hardness with temperature obtained from this study agrees well with the values and trends obtained by Gawrilov [15] for an electroless nickel coating with a 10% phosphorus content, particularly with the maximum hardness reached at a temperature of 400°C. Fig. 4 shows that at heat-treatment temperatures below 400°C the electroless nickel composite coatings have a higher hardness than the electroless nickel coatings, but at 400°C all three coatings have approximately the same hardness value.

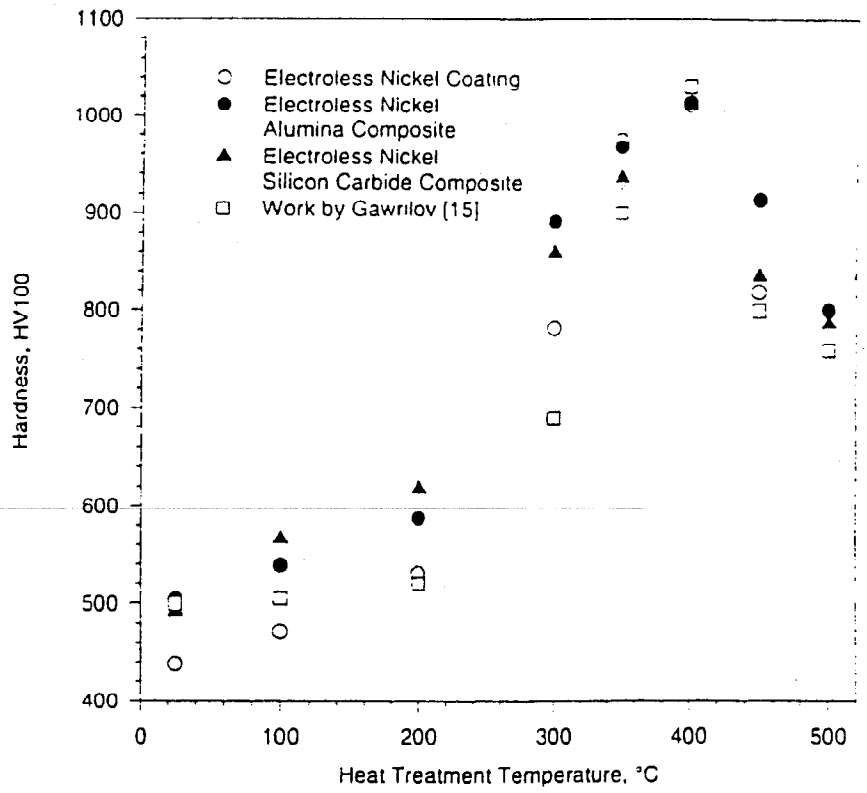

Fig. 4. The hardness of EN coatings as a function of heat treatment temperature.

The increase in hardness of the electroless nickel coating is attributed to the formation of nickel phosphide intermetallic phase [16,17]. Evidence of nickel phosphide and nickel solid solution formation was shown in X-ray diffraction diagrams, where the as-deposited amorphous coatings show a wide intensity peak, but upon heat treatment at temperatures around 250°C several new intensity peaks form and sharpen [2]. The first diffraction peaks to sharpen have been identified to correspond to nickel-rich crystals precipitating from the amorphous parent phase, followed by simultaneous crystallisation of nickel and nickel phosphide. The maximum hardness is reached at a particular temperature approximately where crystallisation of the coating is complete, and above this particular temperature the nickel phosphide particles coarsen and softening occurs.

The hardening mechanism of the coating is believed to be caused by the coherency strain fields surrounding the nickel phosphide particles, i.e. an age-hardening effect, where the nickel phosphide particles are coherent with the nickel-rich matrix. The strain fields act to oppose the movement of dislocations, thus hardening the deposit. However, overaging results in the formation of an incoherent precipitate and a decrease in hardness [2,3].

The electroless nickel composite coatings evaluated in this study showed a higher hardness than the plain electroless nickel coatings (except at 400°C). According to the nickel phosphorus phase diagram, for EN deposits with a phosphorus content of 9–10 wt%, the amount of nickel phosphide is approximately 60 wt% of the deposit. Furthermore the average grain size of nickel phosphide has been reported to be 20–60 Å [18]. For the EN coatings heat treated at 400°C, it appears that the hardening is more due to precipitation than dispersion of ceramic particles.

The hardness measurements obtained in this study are believed to be a fair representation of the bulk hardness of the composite coatings. This confidence is due to the fact that the ENSI400 coating, (with a 20% silicon carbide particle loading by volume), and the ENAL400 coating (loaded with 8% alumina particles by volume), had an interparticle spacing of approximately 4 μm, estimated from figs. 2 and 3. Thus, since the microhardness impressions left by the indenter have diagonal dimensions ranging from 13 to 19 μm, it is certain that the microhardness indenter would have come into contact with several silicon carbide or alumina particles when penetrating the surface of the coating.

In the as-deposited condition, electroless nickel coatings have a hardness of 500 HV100 which is double the hardness of conventional electrolytic nickel coatings. The hardness of the electrodeposited nickel coatings is associated with their fine grain structures and high dislocation densities [8]. The crystalline materials deform by dislocation movement where as the amorphous coatings deform plastically by shear banding, indicating a higher resistance to deformation [6].

3.3. WEAR RESISTANCE

The wear tracks produced by the scratch tester under a constant normal load

were analysed using a profilometer. Fig. 5 shows the variation of scratch depth with applied normal load. The general trend, as expected, is that as the normal load is increased the depth of the scratch increases. Horizontal lines drawn across the plot at 12, 18 and 15 μm correspond to the coating thickness of the ENSI, the ENAL and the EN coatings, respectively. The point where these lines intersect the plot gives a load at which the scratch depth is equal to the coating thickness. These critical loads are shown in table 2 for various coatings. These values indicate that when the coatings are thicker they can withstand higher loads before the indenter reaches the substrate. Also a higher load is required to penetrate the coating containing silicon carbide than any of the other coatings, as evident from the values expressed in load per unit thickness of the coatings.

Fig. 5 shows that the scratch depth varies linearly with the applied load for the steel substrate, while for the coatings straight lines are observed, but with a change in slope at particular loads. It was noted that this transition point corresponds to the load at which the substrate is penetrated.

Fig. 6 shows that the volume of coating material removed increases with increasing load. However, the increase in the volume of material with increasing load is linear, with a point of transition. The points of transition for the different coatings are again similar to the values shown in table 2. These transition points might indicate a change in wear mechanism when these critical load points are reached. Even when

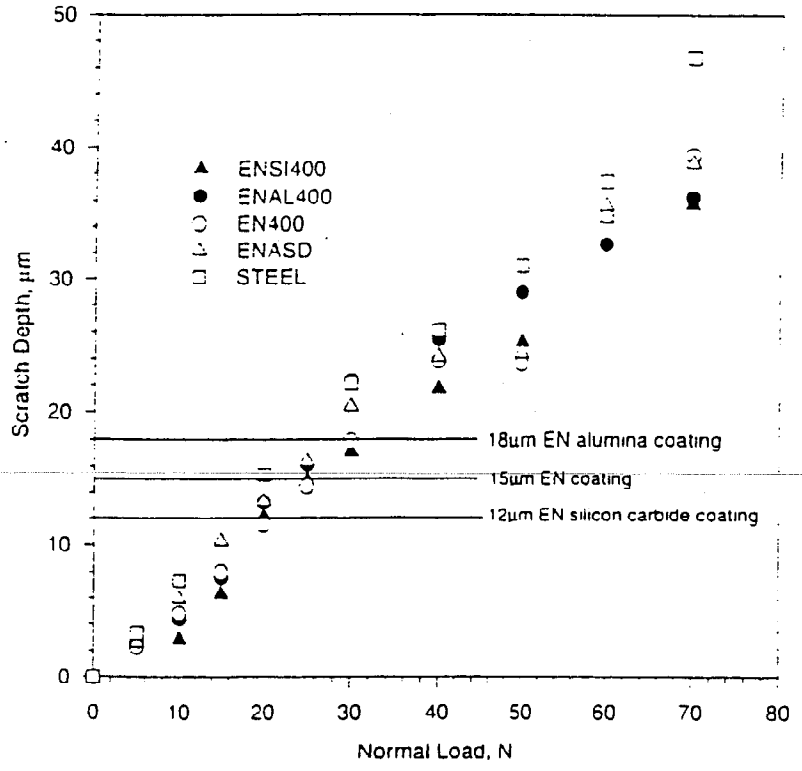

Fig. 5. The scratch depth increases with the normal scratch load.

Table 2
Data comparing the load required to penetrate 1 μm of material

	Coating thickness (μm)	Load when substrate is hit	Load/thickness (N/μm)
ENSI400	12	22	1.83
ENAL400	18	27	1.35
EN400	15	25	1.66
ENASD	15	24	1.6

the indenter penetrates the substrate, the coating would still provide some resistance to abrasive wear.

A bar graph of the volume of material removed from the scratch at a scratch load of 20 N, for each of the four electroless nickel coatings and the steel substrate is plotted in fig. 7. The ENSI400 coating has the smallest volume of material removed from its scratch track, which is three times less compared to the steel substrate at the same load. The other electroless nickel coatings at this load also showed greater wear resistance than the steel substrate.

3.4. SCANNING ELECTRON MICROSCOPY OF SCRATCH TRACKS

The SEM examination of the EN400 and ENAL400 specimens scratched at a

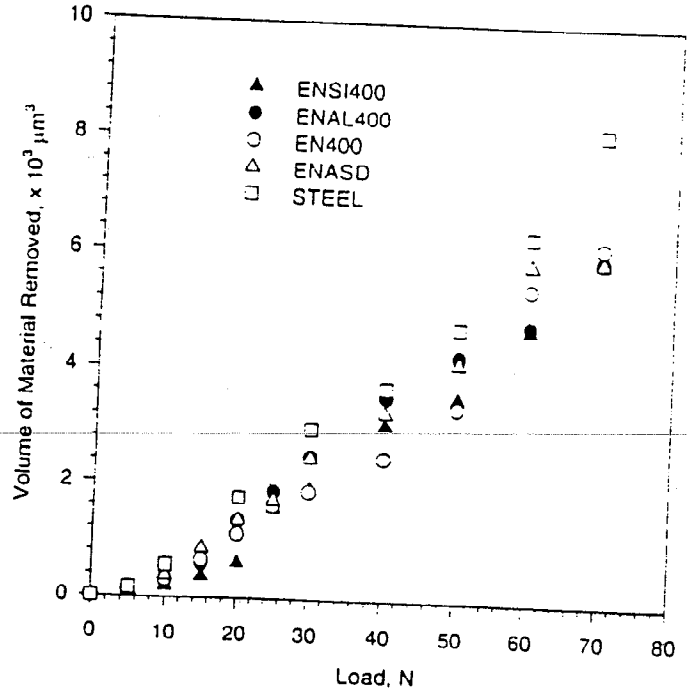

Fig. 6. Volume of coating material removed by scratching as a function of normal load.

10 N load showed cracks had began to form on the edges of the scratch tracks (figs. 8 and 9). The cracks were linear and at an angle of approximately 40–45° to the direction of the scratch. The cracks ran away from the scratch track for 1 mm into the neighbouring coating. However, the ENSI400 coating shows no cracking at all (fig. 10).

The scratch tracks for the as-deposited ENSI, ENAL and EN coatings tested at 10 N loads showed no cracking (figs. 11–13) unlike the heat-treated coatings. The scratch tracks for the as-deposited coatings appeared to be "smeared". The absence of cracks and presence of ductile smearing of the wear tracks for these coatings suggests that electroless nickel coatings are soft and ductile in the as-deposited condition, i.e. they show a high degree of plastic deformation. This observation is supported by the hardness measurements – the as-deposited coatings have a hardness of 500 HV100 compared to 1000 HV100 for the hardened coatings.

At the base of scratch tracks for the hardened coatings tested at a load of 60 N (e.g. ENAl400, fig. 14) tensile cracking was evident and the cracks were in the same direction as described for the as-deposited coatings, but were much finer and more closely spaced. The higher hardness and lower fracture toughness of these heat-treated coatings suggest that they failed in a brittle manner, i.e. by chipping and spallation. This phenomenon was clearly seen in the SEM micrographs of the scratch tracks in this study and is believed to be caused by the large compressive stress generated ahead of the indenter [19]. Generally the heat-treated coatings showed large amounts of chipping as for lower loads, except for the silicon carbide coatings which showed only a small amount of chipping.

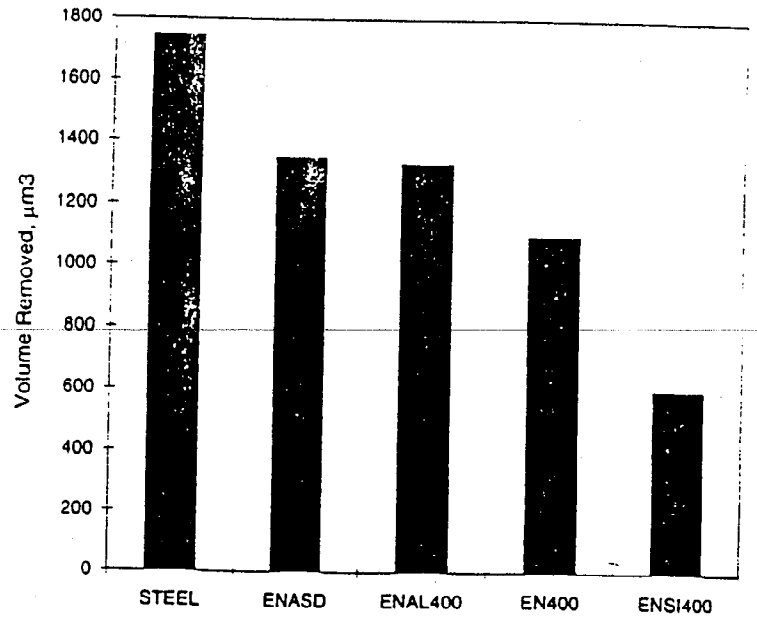

Fig. 7. Volume of coating material removed from scratch tracks of steel EN and EN–ceramic composites at 20 N load.

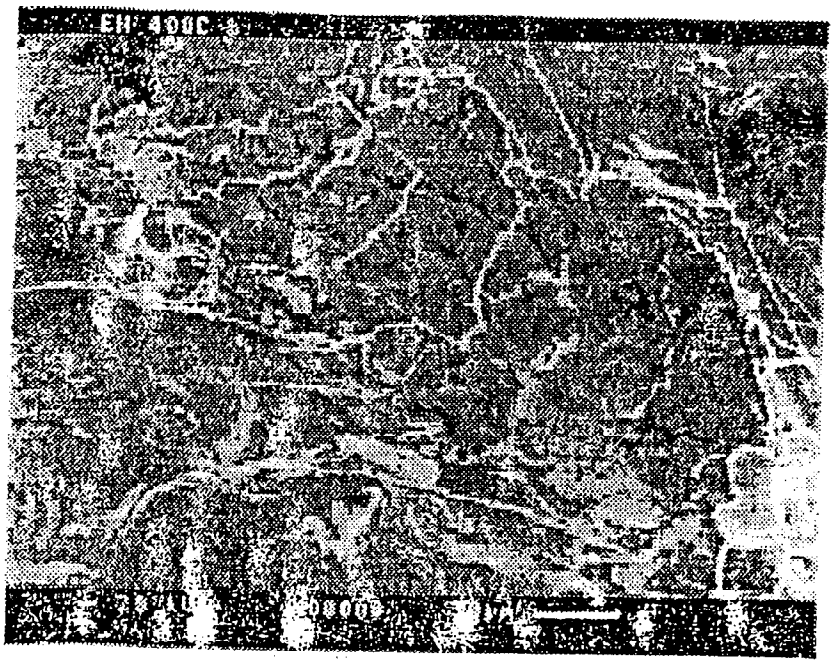

Fig. 8. Scratch track on an EN coating heat treated at 400°C, showing tensile cracking; and cracks propagating into the surrounding coating (10 N load).

The reason why the ENAL400, and EN400 coatings showed more chipping and cracking than the ENSI400 coating (fig. 15) is due to the phosphorus content of the electroless nickel coatings. The phosphorus content of the ENSI coatings was 8%

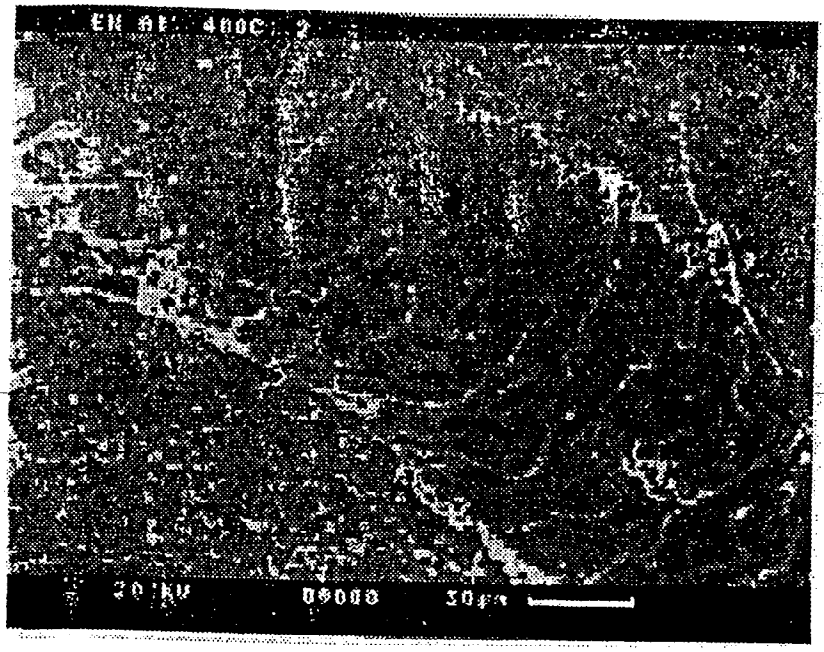

Fig. 9. Scratch track on an EN–alumina coating heat treated at 400°C, showing tensile cracking (10 N load).

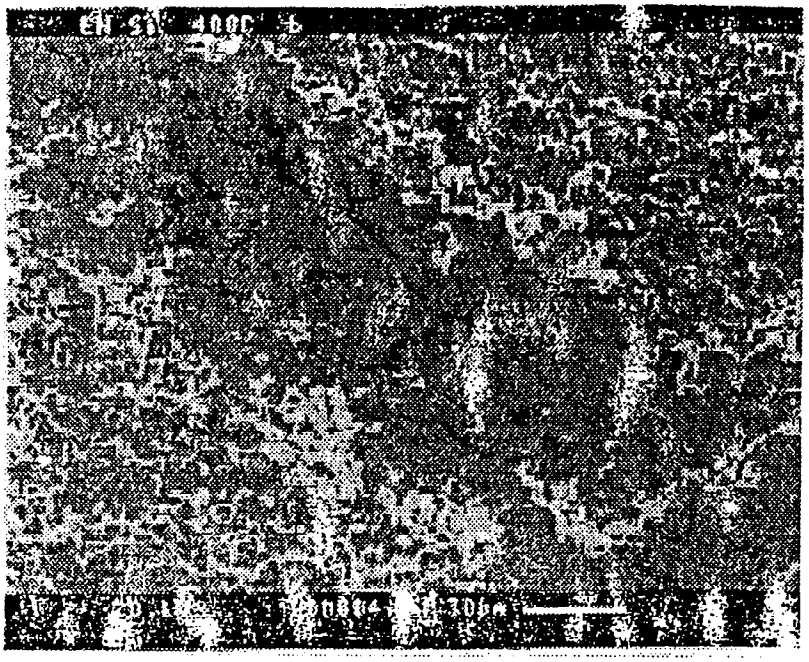

Fig. 10. Scratch track on an EN–silicon carbide coating heat treated at 400°C, with wider spaced tensile cracks and the absence of cracks propagating into the surrounding coating material should be noted (10 N loading).

compared to the ENAL and EN coatings with 10 and 9% phosphorus, respectively. Baldwin and Such have shown that the fracture toughness of the electroless nickel coating decreases substantially when the phosphorus content is raised from 8 to 12% [3].

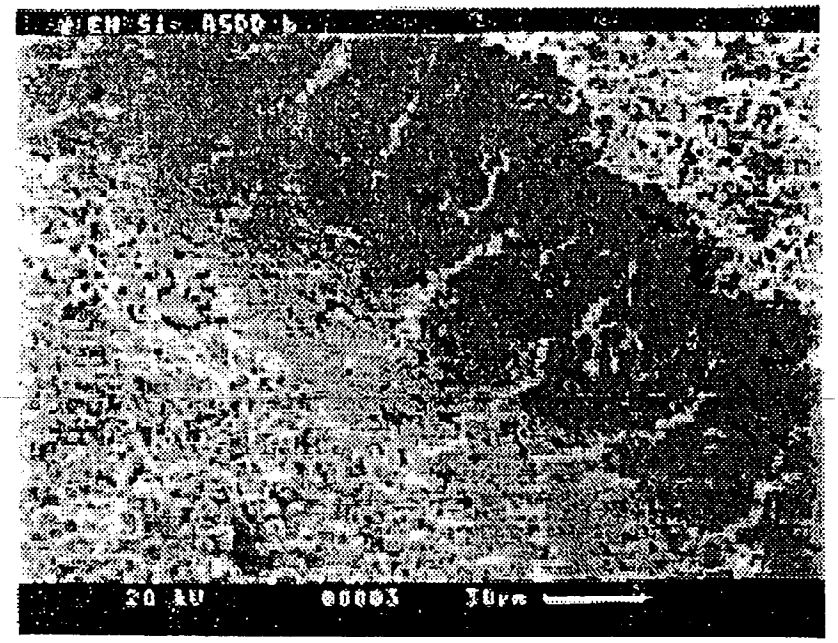

Fig. 11. Scratch track on an as-deposited EN–silicon carbide coating, track shows ductile smearing of coating material (10 N load).

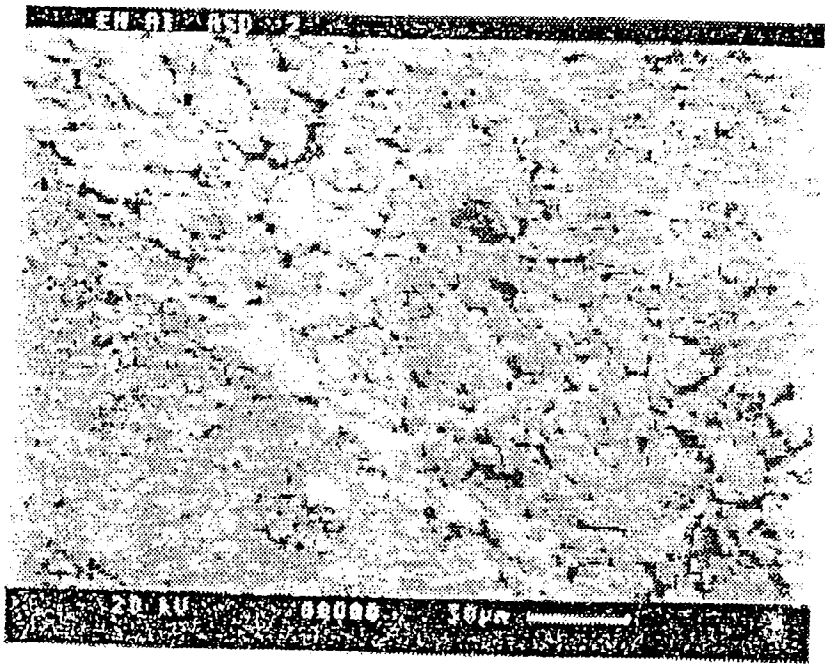

Fig. 12. Scratch track on an as-deposited EN–alumina coating, track shows ductile smearing of the coating (10 N load).

The lower phosphorus content of the ENSI400 coating also means it has less nickel phosphide in its crystallised microstructure, according to the nickel phosphorus phase diagram, i.e. 8% phosphorus is equivalent to 50 wt% nickel phosphide. For the ENAL400 coating it has approximately 70 wt% nickel phosphide in

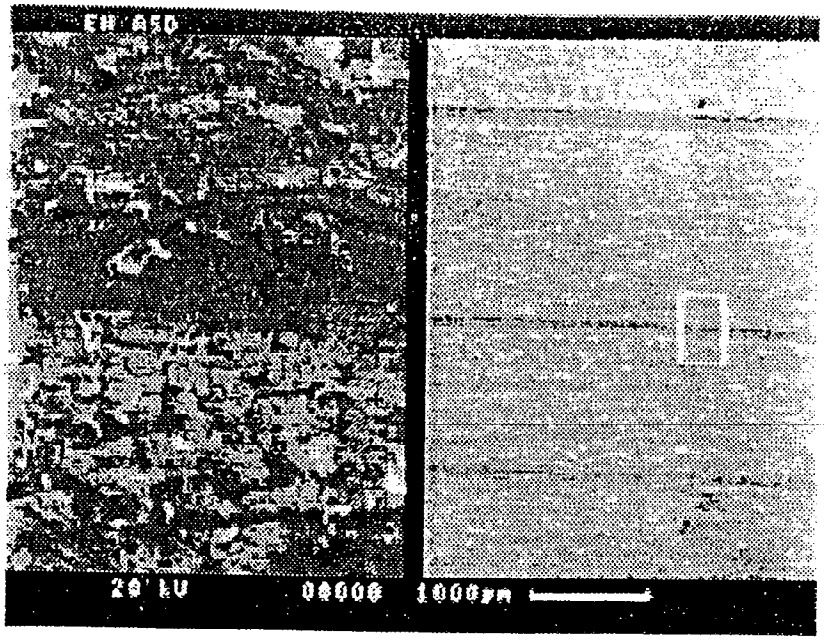

Fig. 13. A composite image showing at low and high magnification the scratch track on an as-deposited EN coating, track shows ductile smearing (10 N load).

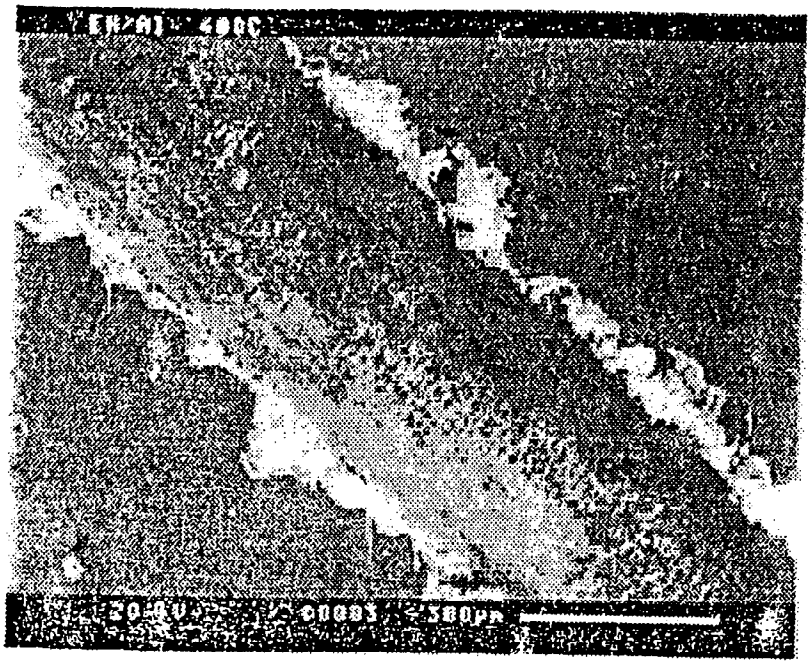

Fig. 14. Scratch track on an EN coating heat treated at 400°C, track shows that at higher scratch loads chipping of the coating at the edges of the scratch track is evident (60 N loading).

its crystallised state. The presence of a larger proportion of nickel phosphide phase results in a coating structure that is harder and lower in fracture toughness. The introduction of hard particles like silicon carbide would tend to increase the hot

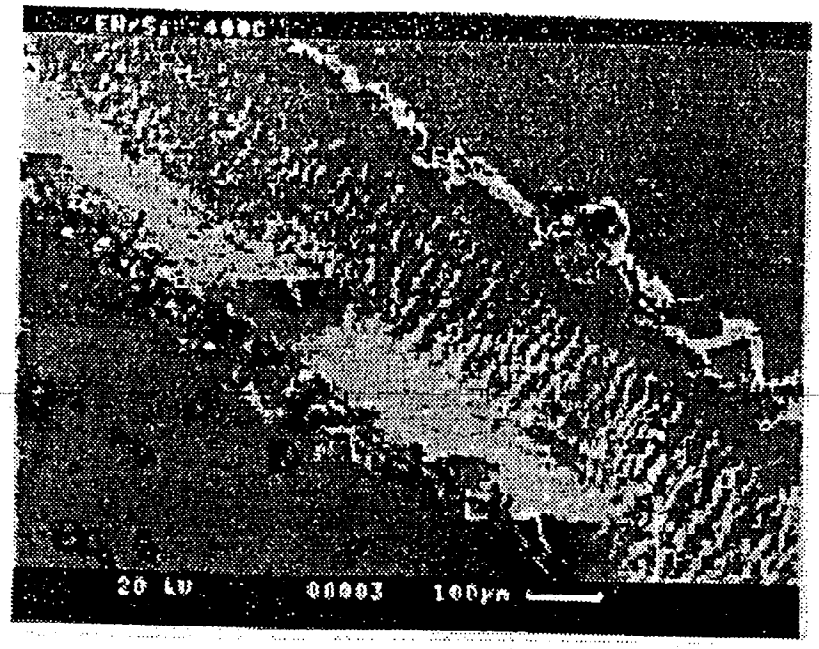

Fig. 15. Scratch track on an EN–silicon carbide coating heat treated at 400°C, at higher loads (60 N) the scratch track shows no sign of chipping or cracking which propagates into the surrounding material.

hardness of the coatings, because unlike the nickel phosphide particles the silicon carbide particles will not coarsen and soften when overaged, and may even prevent grain growth by pinning the grain boundaries.

3.5. WEAR MODEL

An f_{ab} wear model for abrasive wear, developed by Zum Gahr [20], describes the ratio of microcutting to microploughing, or the amount of material loss to the volume of the wear grove. The value of f_{ab} becomes equal to unity for ideal microcutting, equal to zero for ideal microploughing and greater than unity for ideal microcracking (fig. 16). Fig. 17 shows the value of the f_{ab} plotted as a function of the applied load for the ENAL400, ENSI400 and the EN400 coatings respectively. All three graphs show that the f_{ab} ratio increases with load, i.e. at higher loads the volume removed is mainly by microcutting than by microploughing.

For softer materials like steel and the as-deposited EN coatings, the values of f_{ab} were closer to zero indicating that material was removed from the scratch track by a ploughing mechanism. This information, supported by the SEM micrographs of the scratch tracks, throws some light onto the wear mechanisms of electroless nickel coatings.

4. Conclusions

The following conclusions can be drawn based on the study of electroless nickel composite coatings.

(1) The introduction of silicon carbide and alumina particles increased the hardness of the plain electroless nickel coatings at all heat treatment temperatures, except at 400°C where all the coatings tested had the same hardness. It was found that all coatings reached a maximum hardness when heat treated at 400°C of 1008

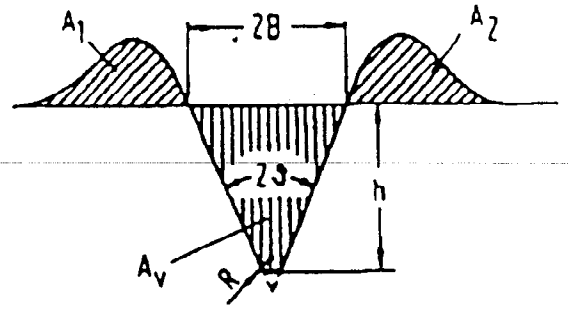

$$f_{ab} = \frac{A_v - (A_1 + A_2)}{A_v}$$

Fig. 16. f_{ab} wear model for abrasive wear, as described by Zum Gahr [20].

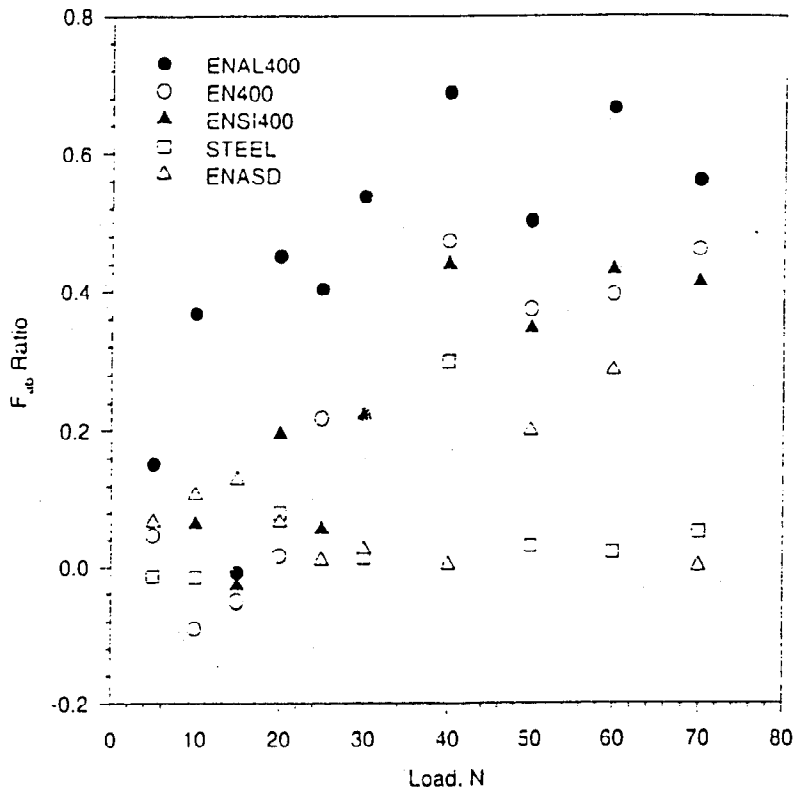

Fig. 17. The f_{ab} value as a function of normal load for the ENAL400 coating, showing that the ENASD coating and the steel substrate suffered wear by microploughing (f_{ab} ratio close to zero), and the ENAL400, EN 400 and ENSI400 coatings changed from microcracking to microploughing wear as the scratch load increased.

HV100. The as-deposited (amorphous) coatings had a hardness of approximately 500 HV100 compared to the substrates hardness of 150 HV100.

(2) The amorphous coatings showed a higher degree of plasticity and fracture toughness than the heat-treated coatings which displayed severe chipping and cracking on the edges of their scratch tracks. The ENSI400 coating, however, was an exception because its phosphorus content was lower, meaning it had a higher fracture toughness than the other heat-treated coatings.

(3) All electroless nickel coatings had a better scratch/wear resistance than the steel substrate, right across the load range tested. The silicon carbide coating had the best scratch resistance of all the coatings, and at 20 N the volume of material removed from its scratch track was 1/3 of the volume removed from the steel substrate.

(4) The as-deposited coatings showed tensile cracking and spallation in the wear tracks and so did the hardened coatings, except the tensile cracks were much finer and more closely spaced.

(5) The use of the f_{ab} ratio indicated that for the heat-treated coatings the wear mechanism changed from microploughing to a microcracking as the scratch load increased.

(6) For the softer as-deposited coatings microploughing was the dominant wea mechanism right across the load range.

(7) It was observed that the increased phosphorus content and hardening of elec troless nickel coatings decreased the fracture toughness of the coatings leading t brittle failure during scratch testing.

References

[1] *ASM Metals Handbook*, Vol 5, Surface Cleaning, Finishing and Coating, 9th Ed. (1982) p. 219.
[2] G. Lu, G. Li and Y. Yu, in: *Proc. Int. Conf. Wear of Materials*, 1985, ed. K.C. Ludem (ASME, New York) p. 382.
[3] T.E. Such and C. Baldwin, Trans. Inst. Metal Finish. 46 (1968) 73.
[4] J.M. Scale, Metal Progress 115 (4) (1979) 74.
[5] D.J. Kenton, Int. J. Powder Metall. Powder Technol. 19 (1983) 185.
[6] D.T. Gawe and U. Ma, Surf. Eng. 4 (1988) 239.
[7] D.T. Gawe and U. Ma, Trans. Inst. Metal Finish. 64 (1986) 129.
[8] D.T. Gawe and U. Ma, Mater. Sci. Technol. 3 (1987) 228.
[9] K. Parker, Plating 61 (1974) 834.
[10] N. Feldstein, T. Lancsek, D. Lindsay and L. Salerno, Metal Finish. 81 (1983) 35.
[11] K. Parker, *Proc. Interfinish 1972*, Basel, p. 202.
[12] H. Wiegard and G. Heinke, Metalloberflache 24 (1970) 163.
[13] J.P. Randin and H.E. Hintermann, Plating 54 (1967) 523.
[14] L.G. Bhatgadde and S. Mahapatra, Metal Finish. 86 (1988) 31.
[15] G.G. Gawrilov, *Chemical (Electroless) Nickel Plating* (Portcullis Press, Redhill, 1979).
[16] K. Parker, Plating Surface Finish. 68 (1981) 71.
[17] H.A. Graham, T.W. Lindsay and H.J. Read, J. Electrochem. Soc. 112 (1965) 401.
[18] C. Ruscior and E. Croiala, J. Electrochem. Soc. 118 (1971) 696.
[19] S.J. Bull, Surf. Coat. Technol. 50 (1991) 25.
[20] K.H. Zum Gahr, Wear 124 (1988) 87.